arXiv:2606.20131v2 [cs.CV] 19 Jun 2026

TriFlow: Generating Artist-Like 3D Mesh Topology via Nearest-Vertex Vector Fields

Haoxuan Li[1], Ziya Erkoç[1], Daniele Sirigatti[2], Vladislav Rosov[2], Lei Li[3], Angela Dai[1], and Matthias Nießner[1]

[1]Technical University of Munich, [2]AUDI AG, [3]University of Virginia

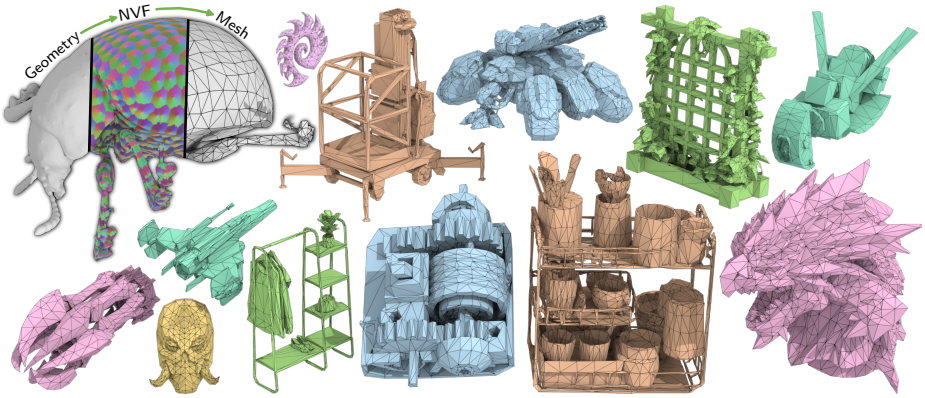


Fig. 1: TriFlow generates high-quality, artist-like mesh topology from input SDFs. **Top Left**: we introduce a nearest-vertex vector field (NVF) to transform discrete topology prediction into efficient, piecewise-continuous field modeling. **Right**: TriFlow robustly generalizes across diverse and complex geometries.

Abstract. We present TriFlow, a new generative approach for producing compact 3D meshes with artist-like triangle topology directly from input geometry conditions such as signed distance fields. Our key insight is to represent mesh topology as a nearest-vertex vector field (NVF) defined over the surface, where each point encodes its association to the nearest triangle vertex in the local barycentric frame. We train a latent flow-matching model to synthesize this field, enabling topology generation conditioned on the input geometry. To extract a coherent mesh, we cluster surface regions using the generated NVF and guide a constrained quadric error metric mesh simplification with topology-aware optimization. This yields output meshes that closely match the input geometry while exhibiting structured, artist-like connectivity. Experiments demonstrate that TriFlow achieves stronger generalization and significantly improved topology quality compared to state-of-the-art learning-based approaches, alongside 90% lower Chamfer Distance and an 8× speedup.

Keywords: 3D Mesh Topology · 3D Generative Mesh Modeling · Mesh Vector Field

1 Introduction

Triangle meshes serve as a fundamental representation across computer graphics and vision, broadly used in surface-based modeling, rendering, animation, physical simulation, 3D reconstruction, digital content creation, and beyond. This prevalence stems from their computational efficiency, explicit surface structure, and direct compatibility with existing production tools. Beyond geometric accuracy, the *topology* of a mesh plays a crucial role: the organization of vertices, edges, and faces strongly influences performance and applicability in downstream applications such as deformation, editing, and simulation; poorly organized connectivity often leads to artifacts and costly manual cleanup. In practice, artists construct meshes with carefully designed topology, which we refer to as *artist-like topology*, characterized by compact face count, smooth vertex distribution, and edge alignment with salient geometric features.

Recent works in 3D generative modeling [4, 19, 31, 32, 61, 63, 64, 66] demonstrate impressive advances in geometry creation. However, the discrete nature of the optimized topologies remains difficult to synthesize directly. These approaches produce high-fidelity geometry as implicit fields, requiring methods like Marching Cubes [38] for mesh extraction, resulting in highly over-tessellated output meshes that are ill-suited for downstream workflows (e.g., real-time game rendering). To address this limitation, recent works have explored generating artist-like meshes directly as discrete triangle sequences in an autoregressive manner [5, 16, 18, 30, 33, 51, 53, 60, 65, 67, 68]. While such methods demonstrate promising results, they suffer from slow token-by-token inference and error accumulation during autoregressive prediction, which often leads to incomplete or low-fidelity generations – limiting their scalability and generalization. A significant gap still exists between high-fidelity 3D geometry modeling and robust, efficient, production-ready mesh topology generation.

To address this, we propose TriFlow, a novel generative approach for creating meshes with artist-like topology. Our key insight is that mesh topology can be represented as a piecewise-continuous field defined over the surface, rather than as discrete connectivity. We thus introduce a nearest-vertex vector field (NVF) that has a bijective mapping to the mesh topology. This representation transforms the task of topology generation into vector-field modeling, thereby avoiding expensive autoregressive sequence modeling. As illustrated in Fig. 1, given input geometry encoded as a signed distance field (SDF), we predict the NVF and then extract a mesh with topology aligned to the field prediction. Our approach is flexible and can handle any inputs that can be represented as SDFs, such as implicit fields from 3D generative methods [47, 64], and fused signed distance grids from sensor measurements [9].

To recover meshes from the generated field, we develop a topology-aware extraction method that first clusters surface regions associated with respective

target vertex positions using a watershed algorithm and then performs constrained quadric error metric (QEM) simplification [17] guided by the predicted targets. This formulation not only preserves geometric fidelity but also effectively captures the topological characteristics in our generated NVF. To enhance robustness against noisy or irregular input geometry commonly encountered in scanning and generative modeling, we introduce randomized surface distortions as data augmentation during training.

Our experiments demonstrate that TriFlow significantly improves topology generation quality and generalization compared to the state of the art [33, 65], while achieving more than 8× speedup. By representing topology as a vector field, our method provides a new perspective on mesh generation that bridges geometry modeling and compact typology extraction. To facilitate reproducibility, we release our complete codebase for training and inference.

In summary, our contributions are:

- We introduce a novel representation of mesh topology using a nearest-vertex vector field (NVF) pointing towards the nearest vertex in the local triangle's barycentric frame.
- We propose a latent flow-matching approach for topology synthesis conditioned on input SDF geometry. We apply random surface distortion during training to enable the model to generalize to noisy or irregular geometry.
- We develop a robust topology-aware mesh extraction approach that combines a watershed algorithm with constrained QEM optimization to produce artist-like mesh outputs from our NVF prediction.

2 Related Work

3D Generation and Reconstruction. 3D generation and reconstruction are highly demanded in practice. Recent generative methods often represent geometry in implicit fields or structured 3D latents, including TRELLIS [63, 64], Direct3D-S2 [61], DORA [4], and recent high-resolution field models [19, 31, 32, 66]. Similarly, reconstruction spans classical volumetric fusion into TSDF/SDF volumes [9,44,45] and neural field modeling such as NeRF [42], NeuS [59], and 3D Gaussian Splatting [27]. Many approaches therefore represent geometry as SDF/occupancy fields or related implicit formulations [40,47]. Meshes are commonly recovered via iso-surfacing [24, 38] or via reconstruction methods [25, 26]. Differentiable and learned extraction variants further improve fidelity [6, 7, 49, 50], yet the resulting meshes are often dense and irregular and do not exhibit production-ready topology for editing and real-time rendering.

Mesh Simplification and Retopology. Given dense proxy meshes, classical geometry processing reduces complexity via edge-collapse decimation, most notably QEM [17] and Progressive Meshes [20]. Several works adapt QEM to achieve the expected collapse behavior required by specific use cases [3,48,57,69]. However, these approaches do not address the need for artist-like topology. On the other hand, production retopology and quadrangulation use direction/cross fields to drive edge flow and patch layout, including N-RoSy design [46], globally

optimal direction fields [28], MIQ [2], Instant Field-Aligned Meshes [23], QuadriFlow [21], and spectral quadrangulation [14]. More recently, learning-based approaches predict or generate such meshing fields, including learned direction fields [12], CrossGen [13], and NeuFrameQ [37]. These quad-meshing pipelines typically favor near-uniform, grid-like layouts, which diverge from artist-like topologies that allocate polygons adaptively to geometric details.

Topology-Aware Mesh Generation. A strong recent trend is to model meshes as discrete sequences. These methods, including PolyGen [43], MeshGPT [51], MeshAnything V2 [5], TreeMeshGPT [33], Nautilus [60], DeepMesh [68], and EdgeRunner [53], Meshtron [18], generate meshes with autoregressive sequence modeling pipelines. Editing, scaling, and LOD-oriented systems include MeshPad [30], MeshMosaic [65], and VertexRegen [67]. While these methods are typically limited by the latency and error accumulation of autoregressive inference, our method bypasses this issue by modeling topology as the NVF.

Flow Matching and Watershed for Surface Segmentation. Flow/rectified-flow objectives provide efficient, simulation-free training and fast sampling in continuous latent spaces [34, 36, 56], and have been adopted in large-scale 3D latent generators [61, 64]. For field-guided surface segmentation, watershed-style clustering is a classical segmentation tool for 2D images [8, 58] and is extended to 3D mesh surfaces [39]. Our method generates the NVF via flow matching and obtains surface clusters using watershed, which serve as topological constraints in the mesh extraction.

3 Method

We introduce a novel generative approach to create compact, artist-like mesh topologies from signed distance field (SDF) inputs. The SDF, denoted as $\mathcal{G}$, is used as the input geometry condition for its flexibility and ease of conversion from other representations. The surface, defined as the zero-level set of the SDF, is represented as $\mathcal{S} \subset \mathbb{R}^3$ containing all surface points.

Our goal is to learn a mapping from $\mathcal{G}$ to an artist-reminiscent mesh $\mathcal{M} = (\mathcal{V}, \mathcal{F})$, where $\mathcal{V} = \{\boldsymbol{v}_i \in \mathbb{R}^3 \mid i = 1, \ldots, N\}$ is the set of vertices, and $\mathcal{F} = \{f_j = (\boldsymbol{v}_{j_1}, \boldsymbol{v}_{j_2}, \boldsymbol{v}_{j_3}) \mid j = 1, \ldots, M\}$ is the set of triangle faces. To efficiently predict the discrete mesh topology, we introduce a nearest-vertex vector field (NVF) to represent mesh connectivity, denoted as $\mathcal{T} = \{\boldsymbol{t}(\boldsymbol{p}) \in \mathbb{R}^3 \mid \forall \boldsymbol{p} \in \mathcal{S}\}$. Our mesh topology generation then follows a two-step pipeline: first generate $\mathcal{T}$ conditioned on $\mathcal{G}$; and then extract mesh $\mathcal{M}$ from the generated $\mathcal{T}$.

An overview of our method is illustrated in Fig. 2. We train a latent flow-matching model to generate the NVF $\mathcal{T}$, conditioned on the SDF latent of the input geometry $\mathcal{G}$. To extract mesh topology, the generated field $\mathcal{T}$ is first clustered via a watershed algorithm to identify regions associated with target mesh vertices. These regions are then used as constraints in the QEM simplification method [17] applied to a proxy mesh representing $\mathcal{G}$ to produce the final output mesh $\mathcal{M}$.

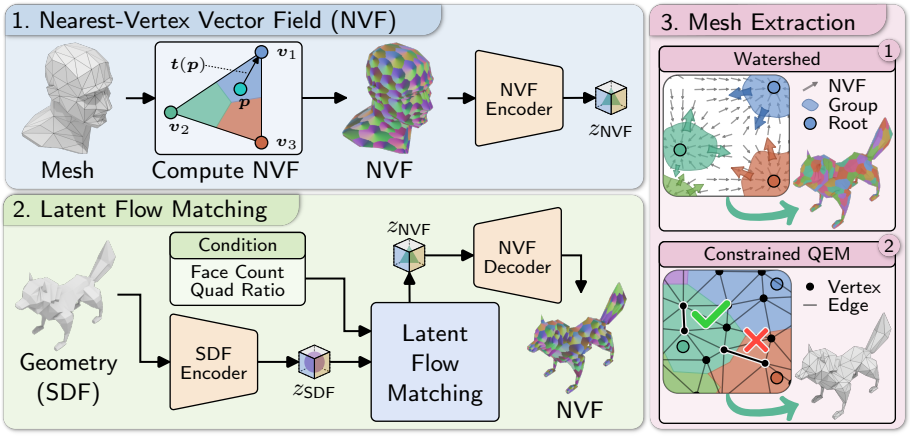


Fig. 2: Method Overview. Our method consists of three major components: **1**. We define the NVF on the surface (local field directions color-coded) to represent the mesh topology; **2**. We train a latent flow-matching network to synthesize the NVF conditioned on the SDF input; **3**. We use the watershed algorithm to cluster the surface and a constrained QEM that only merges vertices in the same group to extract the artist-like mesh as output.

3.1 Nearest-Vertex Vector Field (NVF)

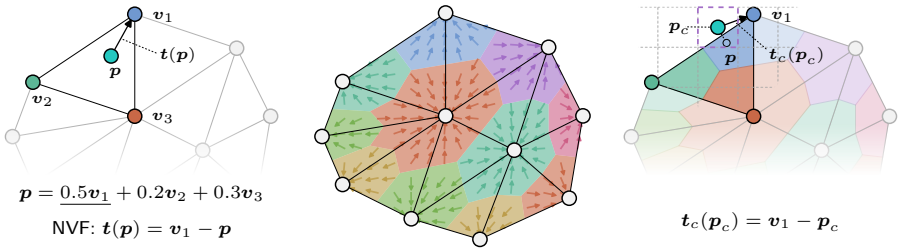
The NVF $\mathcal{T}$ is a vector field defined on the mesh $\mathcal{M}$, as illustrated in Fig. 3a. Given any surface point $\boldsymbol{p} \in \mathcal{S}$, the field value $\boldsymbol{t}(\boldsymbol{p})$ is the vector pointing towards the nearest mesh vertex of $\boldsymbol{p}$ in the local triangle's barycentric frame: $\boldsymbol{t}(\boldsymbol{p}) = \boldsymbol{v}_n - \boldsymbol{p}$, where $\boldsymbol{v}_n$ denotes the nearest vertex. Given the triangle face $f_n = (\boldsymbol{v}_1, \boldsymbol{v}_2, \boldsymbol{v}_3)$ containing the point $\boldsymbol{p}$, we build a barycentric coordinate system and represent $\boldsymbol{p}$ as $\boldsymbol{p} = \lambda_1\boldsymbol{v}_1 + \lambda_2\boldsymbol{v}_2 + \lambda_3\boldsymbol{v}_3$, where $(\lambda_1, \lambda_2, \lambda_3)$ are the barycentric coordinates satisfying $\lambda_i \geq 0$ and $\lambda_1 + \lambda_2 + \lambda_3 = 1$. The nearest vertex index is determined by

$$n = \arg \max_{i \in \{1,2,3\}} \lambda_i, \tag{1}$$

which assigns $\boldsymbol{p}$ to the vertex with the maximal barycentric weight in the local triangle.

To enable efficient generative modeling, we discretize the surface $\mathcal{S}$ and the NVF $\mathcal{T}$ into a sparse voxel grid. As shown in Fig. 3c, for each voxel intersecting with $\mathcal{S}$, we take the voxel center $\boldsymbol{p}_c$ and find its nearest point $\boldsymbol{p}$ on the surface and the triangle f_n containing $\boldsymbol{p}$. Then Eq. (1) is used to determine the nearest vertex $\boldsymbol{v}_n$. The voxelized NVF at this voxel is defined as $\boldsymbol{t}_c(\boldsymbol{p}_c) = \boldsymbol{v}_n - \boldsymbol{p}_c$.

This representation partitions each triangle into three regions corresponding to its incident vertices, implicitly encoding topology. Points mapped to the same triangle vertex form a connected surface region, with region adjacency corresponding to the mesh vertex connectivity, as shown in Fig. 3b. Unlike the



(a) Definition **(b)** Surface NVF **(c)** Sparse Voxelization

Fig. 3: Definition of the nearest-vertex vector field (NVF). **(a)** The NVF is defined as a vector pointing towards the vertex with the largest barycentric weight. **(b)** The NVF defines surface regions whose connectivity aligns with the vertex connectivity. **(c)** We voxelize the NVF for neural network training.

discrete vertex-face representation $(\mathcal{V}, \mathcal{F})$, the NVF is piecewise continuous and suitable for neural modeling.

3.2 Latent Flow-Matching Model for NVF

We learn to generate mesh topology by predicting the latent representation of the NVF $\mathcal{T}$, conditioned on the input SDF $\mathcal{G}$. As shown in Fig. 2, the model takes as input an SDF latent z_{SDF} representing $\mathcal{G}$, together with user-controlled topology parameters, and generates a latent z_{NVF} to be decoded into the NVF.

SDF Condition Encoding. We voxelize the input SDF $\mathcal{G}$ on a 512^3 grid and discard voxels with unsigned distances greater than $1/128$ of the maximum extent of its bounding box, resulting in a sparse voxel representation. We train an autoencoder that encodes the SDF grid into a sparse latent grid z_{SDF} of resolution 64^3. The model is trained with an ℓ_1 reconstruction loss: $\mathcal{L}_{\text{SDF}} = \|\hat{\text{SDF}} - \text{SDF}\|_1$. The resulting latent serves as a compact geometric condition for generating mesh topology.

NVF Encoding and Decoding. The NVF $\mathcal{T}$ is voxelized at resolution 512^3 and encoded using a variational autoencoder (VAE) into a sparse latent grid z_{NVF} of size 64^3. We parameterize the field $\mathcal{T}$ using its unit direction $\boldsymbol{d} = \mathcal{T}/\|\mathcal{T}\|_2$ and the square root of its magnitude $s = \sqrt{\|\mathcal{T}\|_2}$, which are the direct output of the decoder. This decomposition prioritizes directional consistency in low-magnitude regions near mesh vertices, which is critical for accurate mesh extraction. We train the model using an ℓ_1 loss on the reconstructed direction $\hat{\boldsymbol{d}}$ and scaled magnitude $\hat{s}$, alongside a KL-divergence loss weighted by λ_{KL}:

$$\mathcal{L}_{\text{NVF}} = \|\hat{\boldsymbol{d}} - \boldsymbol{d}\|_1 + \|\hat{s} - s\|_1 + \lambda_{KL}\mathcal{L}_{KL}. \tag{2}$$

Latent Flow Matching. Given the SDF latent z_{SDF} and topology control parameters consisting of the target face count and quad-face ratio, which control the output mesh density and topological regularity, we train a latent flow-matching network [64] to generate the NVF latent z_{NVF}. Training is performed

along a linear interpolation path between a ground-truth latent z_0 and Gaussian noise ϵ,

$$z(i) = (1 - i)z_0 + i\epsilon, \quad i \in [0, 1], \tag{3}$$

which progressively transforms data samples into noise. The network learns a time-dependent velocity field u that moves samples along this path toward the data distribution. The training follows the conditional flow-matching objective:

$$\mathcal{L}_{\text{flow}} = \mathbb{E}_{i,z_0,\epsilon}\left[\|u_\theta(z(i), i, z_{\text{SDF}}, c) - (\epsilon - z_0)\|_1\right], \tag{4}$$

where c denotes the topology control parameters. The generated latent is finally decoded to obtain the voxelized NVF $\mathcal{T}$.

3.3 Mesh Extraction from NVF

To mitigate clustering ambiguity caused by prediction uncertainty, we first process the predicted NVF to obtain a spatially smooth field, ensuring that surface points are robustly grouped into consistent components. The topology intrinsic to the surface grouping is then transferred to a mesh as output. This process is also constrained by optimization objectives in accordance with QEM for geometry alignment.

NVF Smoothing and Transfer. Given the voxelized NVF prediction from the flow-matching model, we first apply a bilateral filter to suppress noise in locally smooth regions inferred by the network. We extract an over-tessellated mesh $\mathcal{M}_d = (\mathcal{V}_d, \mathcal{F}_d)$ from the SDF $\mathcal{G}$ using marching cubes [38] as a proxy whose vertices densely sample the surface of $\mathcal{G}$. We then transfer the voxelized NVF onto the vertices of $\mathcal{M}_d$ as follows. For each vertex $\boldsymbol{v}_d$ in $\mathcal{M}_d$, we locate its nearest voxel center $\boldsymbol{p}_{c_n}$ and assign an NVF vector according to

$$\boldsymbol{t}_d(\boldsymbol{v}_d) = \boldsymbol{v}_n - \boldsymbol{v}_d, \qquad \boldsymbol{v}_n = \boldsymbol{p}_{c_n} + \boldsymbol{t}_c(\boldsymbol{p}_{c_n}), \tag{5}$$

where $\boldsymbol{t}_c(\boldsymbol{p}_{c_n})$ denotes the predicted NVF at the voxel center. This assignment ensures that the vector associated with $\boldsymbol{v}_d$ points toward the same target position indicated by the corresponding voxel prediction.

Watershed Algorithm. Ideally, the NVF naturally groups surface points $\mathcal{S}$ into distinct clusters, where points in the same cluster share a common target vertex (Fig. 3b). However, in practice, prediction noise and voxelization artifacts can cause clustering ambiguity. To robustly recover the connected components defined by the NVF prediction, we introduce a watershed algorithm that iteratively expands regions on the surface of $\mathcal{M}_d$. The algorithm consists of the following three steps:

1) Region Root Initialization. Region roots are defined as vertices in $\mathcal{V}_d$ with small predicted displacement magnitudes, indicating they are spatially close to a target mesh vertex:

$$\mathcal{R} = \{\boldsymbol{r} \in \mathcal{V}_d \mid \|\boldsymbol{t}_d(\boldsymbol{r})\|_\infty \leq \tau\}, \tag{6}$$

where τ is a threshold. Each root seeds an initial cluster.

2) Iterative Region Expansion. Let $\boldsymbol{x}(\boldsymbol{v}_d) = \boldsymbol{v}_d + \boldsymbol{t}_d(\boldsymbol{v}_d)$ denote the predicted target position for a vertex $\boldsymbol{v}_d \in \mathcal{V}_d$. Starting from the region roots, cluster labels are propagated over the mesh adjacency graph of $\mathcal{M}_d$ using a priority queue, iteratively growing the seed regions. At each step, an unlabeled neighboring vertex joins the cluster of the root $\boldsymbol{r} \in \mathcal{R}$ that offers the closest predicted target position in Euclidean distance:

$$\text{cost}(\boldsymbol{v}_d, \boldsymbol{r}) = \|\boldsymbol{x}(\boldsymbol{v}_d) - \boldsymbol{x}(\boldsymbol{r})\|_2 . \tag{7}$$

Vertices are processed in ascending order of this cost, producing a watershed-like expansion that favors spatially coherent regions.
3) Updating NVF. Once all vertices are assigned to clusters, we update the NVF on $\mathcal{M}_d$ according to the predicted position of region roots:

$$\boldsymbol{t}_d(\boldsymbol{v}_d) \leftarrow \boldsymbol{x}(\boldsymbol{r}) - \boldsymbol{v}_d. \tag{8}$$

Constrained QEM. While the NVF captures the desired artist-like connectivity, the predicted vertex positions often exhibit small misalignments with $\mathcal{G}$. To achieve high geometric fidelity, we "snap" the topology to $\mathcal{G}$ via a geometry-aware optimization. Therefore, we utilize the proxy mesh $\mathcal{M}_d$ for the geometry $\mathcal{G}$. Optimizing $\mathcal{M}_d$ by combining topology constraints derived from the NVF and the vanilla QEM quadrics results in a mesh aligned to both the intended topology and the original geometry $\mathcal{G}$. The vanilla QEM simplifies a mesh by iteratively collapsing vertex pairs while maintaining surface error approximations using quadric matrices. Each vertex is associated with a symmetric 4×4 matrix Q_{geom} that encodes the incident triangle set. Each edge is assigned a cost computed from the vertex quadrics, measuring the geometric distortion induced by collapsing the edge. Edges with costs below a certain threshold are collapsed to obtain a simplified mesh while preserving the overall geometry. However, the vanilla QEM does not faithfully respect artist-like mesh topology.

Our key idea is to restrict edge collapses according to the predicted topology. Specifically, an edge collapse is rejected if the two vertices have different region roots, as determined by the watershed algorithm. This prevents undesirable merging of distinct regions and aligns the resulting topology with the NVF prediction. When a valid edge collapse involves root vertices, we bias the resulting contraction point toward the corresponding vertex position predicted by the generative model. We achieve this by augmenting the geometric quadric with an additional positional constraint Q_t. The resulting quadric is defined as

$$Q = \text{mean}(Q_{\text{geom}}) + \lambda_t Q_t, \quad Q_t = \begin{bmatrix} 1 & 0 & 0 & -x_t \\ 0 & 1 & 0 & -y_t \\ 0 & 0 & 1 & -z_t \\ -x_t & -y_t & -z_t & \|\boldsymbol{x}(\boldsymbol{v}_d)\|_2^2 \end{bmatrix}, \tag{9}$$

where $\text{mean}(Q_{\text{geom}})$ denotes the average geometric quadrics accumulated at the two vertices of the edge, Q_t is a quadratic penalty encouraging the vertex position to remain close to the target $\boldsymbol{x}(\boldsymbol{v}_d) = (x_t, y_t, z_t)^\intercal$, and λ_t controls the constraint strength.

3.4 Geometric Data Augmentation

To improve robustness against noise and irregularity common in generated or scanned geometry, we apply a random 3D distortion field to the training data. By randomly perturbing the geometry and its corresponding NVF fields, we force the model to learn stable topological predictions even in the presence of significant local surface noise or geometric distortions. More details, including the definition of the distortion field, are provided in the supplementary material.

4 Experiments

4.1 Implementation Details

The training dataset contains 656k Objaverse [11] samples. The SDF autoencoder is built from fine-tuning the VAE of Direct3D-S2 [61] for 170k iterations with a batch size of 16 on 8×A6000 GPUs for 8 days. The NVF VAE adopts the same architecture, and is trained with $\lambda_{\mathrm{KL}} = 0.001$ for 252k iterations with batch size 32 on 8×H100 GPUs for 11 days. The latent dimension of both SDF and NVF is 16. We build our conditional latent flow matching model based on the TRELLIS [64] architecture. The model is trained for 179k iterations with a batch size 64 on 8×H100 GPUs for 12 days. All evaluations and runtime measurements are conducted on a single A6000 GPU with 4 CPU cores. Please refer to the supplementary material for more details.

4.2 Metrics and Baselines

Evaluation Metrics. We evaluate both geometric fidelity and topological quality using complementary metrics. Geometric accuracy is evaluated using Chamfer Distance between the input and output surfaces after normalizing meshes to a unit cube. We uniformly sample 10k surface points from each mesh to compute the distance. We report Fréchet Inception Distance (FID) between shaded renderings of generated and ground-truth meshes to quantify visual geometric similarity. Additionally, we introduce perceptual ratings from vision-language models (VLMs) [54, 55] on mesh geometry and topology to evaluate the visual coherency with artist-created meshes. We also let VLMs compare wireframe renderings and report pairwise preferences of our method against baseline methods. We further conduct a human perceptual study where participants rate and compare outputs from different approaches.

Baselines. We compare against both classical mesh simplification methods and recent learning-based approaches. Classical baselines include vanilla QEM [17,70] and QuadriFlow [1, 21], which represent widely used geometry-driven mesh simplification and remeshing techniques. We also include TreeMeshGPT [33] and MeshMosaic [65] as state-of-the-art learning-based methods that model priors of artist-created topology. Together, these baselines enable a comprehensive evaluation of topology quality, geometric preservation, and generalization.

Table 1: Quantitative comparison with state of the art on Objaverse [11] and TRELLIS [64]-generated shapes. Chamfer Distance is scaled by a factor of 1000. $\{\mathrm{M}, \mathrm{U}\}_{\{\mathcal{G},\mathcal{T}\}}$ represents perceptual scores of geometrical similarity and topological likeness to artist meshes provided by VLMs (M) and human volunteers (U), respectively. Our method consistently outperforms baselines in both geometric similarity and topological quality.

	Objaverse [11]				**TRELLIS [64] Geometry**					
Method	**CD↓**	**FID↓**	$\mathbf{M}_{\mathcal{G}}\uparrow$	$\mathbf{M}_{\mathcal{T}}\uparrow$	**CD↓**	**FID↓**	$\mathbf{M}_{\mathcal{G}}\uparrow$	$\mathbf{M}_{\mathcal{T}}\uparrow$	$\mathbf{U}_{\mathcal{G}}\uparrow$	$\mathbf{U}_{\mathcal{T}}\uparrow$
QEM [17]	0.14	8.0	4.3	3.3	**0.20**	22.1	3.6	3.3	4.0	3.6
QuadriFlow [21]	4.81	46.9	3.0	2.7	0.52	95.6	3.4	3.1	2.5	3.2
MeshMosaic [65]	1.62	27.0	3.9	3.6	9.02	45.3	2.8	1.7	3.3	2.1
TreeMeshGPT [33]	0.98	8.1	3.8	3.5	30.00	74.9	1.9	1.7	1.5	1.7
Ours	**0.12**	**5.0**	**4.8**	**4.7**	**0.20**	**16.2**	**4.4**	**4.0**	**4.5**	**4.6**

4.3 Experimental Setup

Evaluation Data. We conduct evaluation on two datasets. The first consists of $\sim$ 1000 test samples from Objaverse [11], chosen to guarantee single-component meshes with clean, artist-like topology. The second dataset contains 65 shapes generated by TRELLIS [64], which exhibit challenging geometries with artifacts commonly observed in generative approaches, such as bumpy surfaces. Evaluation on TRELLIS data demonstrates the practicality and generalization of our method in real-world 3D content creation pipelines.
Target Face Counts. For Objaverse samples, we set the target number of faces for all capable methods — including Ours, QEM, and QuadriFlow — to match the ground-truth mesh. For TRELLIS samples, we set the target to $\sim$ 6000 faces.
Method-Specific Settings. For the part-based baseline MeshMosaic [65], Objaverse shapes are treated as single-part meshes. Following their recommended pipeline, TRELLIS shapes are decomposed into 20 parts using PartField [35]. QuadriFlow requires manifold meshes as input, and thus non-manifold samples are excluded when computing evaluation metrics for QuadriFlow to ensure a fair comparison. We use the target quad-face ratio of 0.95, the root threshold τ as $1/2$ voxel size, and the topology weight $\lambda_t = 0.1$ in our method. The impact of these parameters is discussed in the supplementary material.

4.4 Comparison to State of the Art

We compare TriFlow against classical approaches and learning-based methods on Objaverse [11] and TRELLIS [64]-generated shapes. Objaverse serves as an in-domain benchmark, as the learning-based methods are trained on its distribution. In contrast, TRELLIS-generated shapes provide out-of-distribution validation, serving as a practical test of converting over-tessellated 3D generations to compact, production-ready mesh structures. Quantitative results are summarized in Tab. 1, perceptual preference studies are reported in Tab. 2, and qualitative comparisons are shown in Fig. 4.

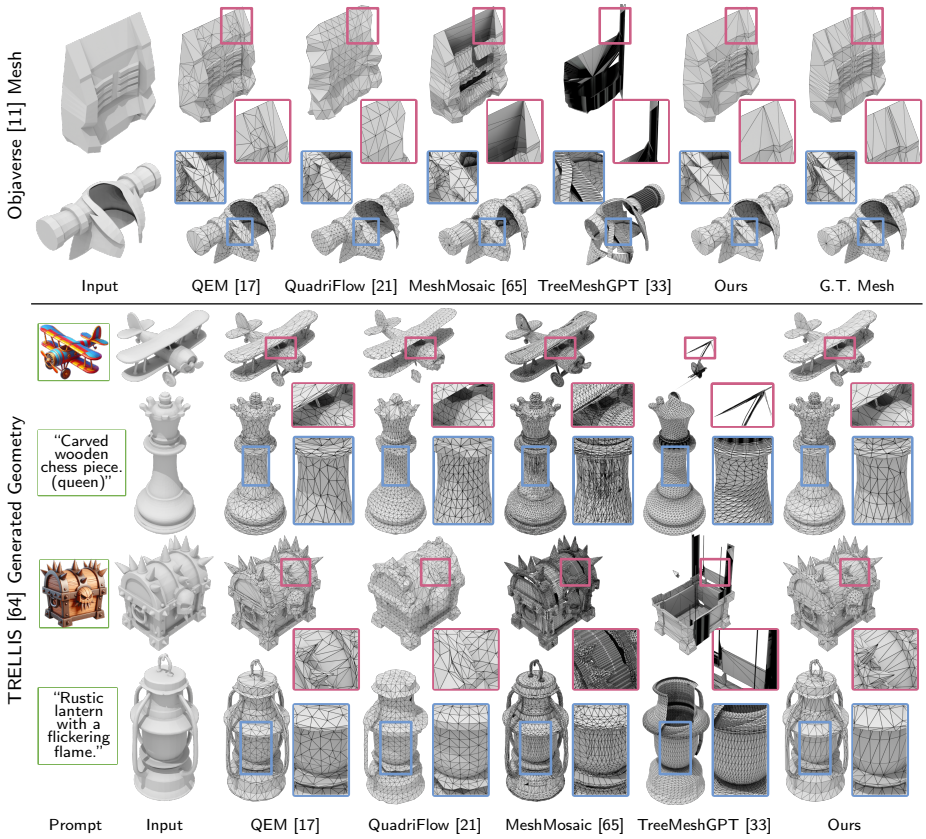


Fig. 4: Visual Comparison. TriFlow demonstrates superior robustness across diverse input geometries. We specifically evaluate on outputs from TRELLIS [64] to simulate a practical production pipeline, where raw generative outputs with over-tessellated meshes require conversion into clean topology. Our approach consistently produces high-quality, artist-like topologies characterized by compact triangles and regular edge flows, while maintaining high fidelity to the original geometry.

Overall, TriFlow consistently outperforms prior approaches: across TRELLIS shapes and Objaverse, our method obtains either the best or tied-best Chamfer Distance while simultaneously achieving the lowest FID and the highest perceptual geometry and topology scores. The preference study in Tab. 2 further supports this trend, where both VLM-based evaluation and human judgments consistently favor meshes produced by TriFlow across geometry, topology, and overall preference.

A notable observation is the limited generalizability of learning-based baselines when evaluated beyond their training distribution, denoted by their performance gap between Objaverse and TRELLIS shapes in Tab. 1. We attribute this to two fundamental design limitations. First, these approaches represent meshes as ordered token sequences. As a result, a significant portion of model capac-

Table 2: Perceptual preferences of our method compared to baselines, based on VLMs and human participants. Our method is consistently preferred in both geometry and topology quality.

Ours vs.	**QEM** [17]	**QuadriFlow** [21]	**MeshMosaic** [65]	**TreeMeshGPT** [33]
VLM-Geometry	70.7%	81.8%	93.0%	82.9%
VLM-Topology	65.9%	84.8%	74.4%	92.7%
VLM-Preference	68.3%	84.8%	76.7%	92.7%
Human-Geometry	76.5%	95.7%	84.4%	97.9%
Human-Topology	80.2%	94.9%	96.1%	95.0%
Human-Preference	83.3%	97.1%	90.8%	97.9%

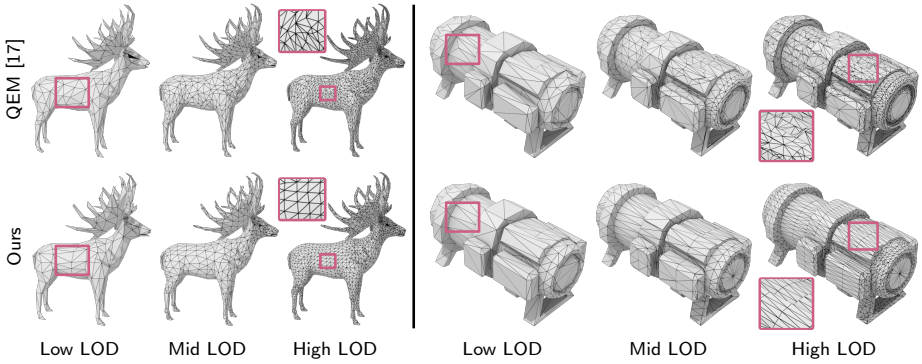
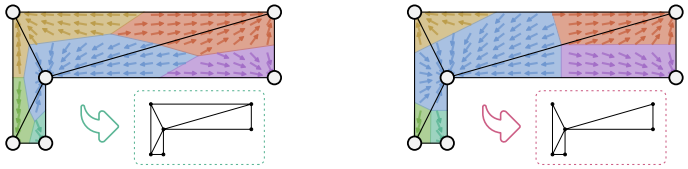


Fig. 5: LOD comparison. Our method produces regular and efficient triangle layout across multiple LODs, while QEM results in irregular triangle soup with the same triangle count budget.

ity is spent on modeling sequence ordering, reducing the effective capacity for modeling geometric and topological relations. Second, autoregressive generation introduces accumulated errors: under out-of-distribution inputs such as TRELLIS geometry, errors accumulate faster, leading to more failures, as reflected in Fig. 4. In contrast, TriFlow avoids sequential dependency during generation, enabling more stable predictions and consistent performance across both datasets.

Level-of-Detail (LOD) Topology. Level-of-detail (LOD) is required in modern graphics pipelines, where meshes must remain visually consistent under varying computational budgets and viewing distances. We therefore evaluate TriFlow's performance across multiple simplification levels and compare it with QEM [17]. As shown in Fig. 5, TriFlow excels in shape abstraction at low LODs, producing regular edge flows that mirror the desirable topology of artist-crafted low-poly models. At higher resolutions, TriFlow yields a dense, structured tessellation characteristic of artist-like polygonal modeling. While QEM offers competitive shape preservation, it produces highly irregular triangular meshes that may pose challenges to downstream editing and lead to artifacts in rendering pipelines. In contrast, TriFlow introduces a learned topology prior without



(a) Using Barycentric Coordinates **(b)** Using Euclidean Distance

Fig. 6: Analysis of using barycentric weights in NVF. This simple example shows that defining a nearest-vertex vector field with barycentric weights **(a)** faithfully represents the topology, compared to the naive Euclidean distance **(b)**.

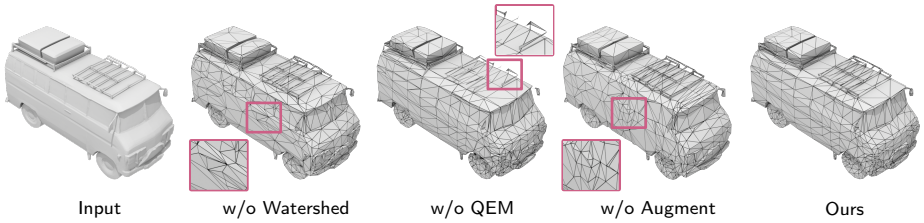


Fig. 7: Ablation Study. Results highlight the impact of our three main contributions: watershed algorithm for topological alignment to the prediction; constrained QEM for geometry preservation; and data augmentation for robustness.

compromising geometric fidelity, providing LOD meshes that feature both well-preserved geometry and optimized topology.

Runtime. While autoregressive learnable baselines are capable of generating a large amount of triangles, they are fundamentally limited by the latency of token-by-token generation. Consequently, processing a single sample takes 2.2 hours with MeshMosaic [65] and 4.3 minutes with TreeMeshGPT [33]. In contrast, by representing topology as a vector field, TriFlow achieves significantly accelerated generation: processing a sample takes only 31 seconds.

4.5 Ablations

We ablate design choices and individual contribution components of our pipeline, covering NVF formulation, watershed grouping, QEM optimization, and geometric data augmentation.

Defining NVF with Barycentric Frames. We first analyze our NVF formulated with barycentric coordinates vs. Euclidean distances. As illustrated in Fig. 6, computing nearest vertices naively by Euclidean distance fails to respect mesh connectivity, particularly for structures like those in Fig. 6.

Watershed Grouping Enforces Topology Alignment. We ablate the watershed algorithm and apply constrained QEM to NVF predictions by directly adding positional quadrics Q_t to all vertex quadrics in QEM. This penalizes large displacements between vertices $\boldsymbol{v}_d$ and their predicted target positions $\boldsymbol{x}(\boldsymbol{v}_d)$ (Sec. 3.3). The QEM is also performed without rejecting edge collapse across

Table 3: Ablations on TRELLIS [64] Geometries. The Chamfer Distance is scaled by a factor of 1000. $M_{\{\mathcal{G},\mathcal{T}\}}$ represents perceptual scores of geometrical similarity and topological preference to artist meshes provided by VLMs. Removing any key component of our approach results in a performance degradation.

Method	CD↓	FID↓	$M_{\mathcal{G}}$↑	$M_{\mathcal{T}}$↑
w/o Watershed	0.21	25.95	3.9	3.8
w/o QEM	0.21	29.13	4.1	3.5
w/o Augmentation	**0.20**	18.06	4.2	3.7
Ours	**0.20**	**16.19**	**4.4**	**4.0**

watershed groups. Tab. 3 (w/o Watershed) shows performance degradation in geometric and topological quality, and Fig. 7 visualizes the irregular triangulation, confirming the utility of the watershed algorithm in enforcing topology alignment to the network prediction.

Constrained QEM Prevents Topological Artifacts and Enforces Geometry Preservation. Replacing the constrained QEM optimization with a naive iterative vertex-flow (driven solely by the NVF) results in significant topological artifacts and discontinuities (Tab. 3 w/o QEM). As shown in Fig. 7, the absence of geometric constraints leads to "missing" geometry, highlighting the necessity of geometric constraints during mesh extraction.

Geometric Data Augmentation Enables Robust Generalization. Without the distortion augmentation, the trained model fails to generalize to local surface variations (Tab. 3 and Fig. 7, w/o Augmentation), leading to a failed topology prediction in those regions.

Limitations. The primary limitation of our approach is the reliance on a voxelized representation, which poses challenges for scaling to large-scale scenes. Future work could address this by adopting a multi-resolution, coarse-to-fine generation strategy or a chunk-based pipeline to enable efficient artist-like topology generation of expansive 3D environments.

5 Conclusion

In this paper, we present TriFlow, a generative approach that models mesh topology as a nearest-vertex vector field to enable structured mesh generation from geometric observations. By representing topology as a piecewise continuous field rather than a discrete sequence, our approach avoids the high computational costs and error accumulation issues in autoregressive mesh generation methods. Experiments show that TriFlow achieves state-of-the-art performance in producing compact, artist-like topology while maintaining high geometric fidelity at low computational cost, demonstrating improved generalization over prior learning-based baselines. We believe this work provides a new perspective on bridging the gap between neural geometry synthesis and the topological requirements in practical 3D creation workflows.

Acknowledgements

This work was funded by AUDI AG. Angela Dai was supported by the ERC Starting Grant SpatialSem (101076253) and Matthias Nießner by the ERC Consolidator Grant Gen3D (101171131). We thank Rui Xu for assistance in running MeshMosaic.

References

1. Blender Online Community: Blender - a 3D modelling and rendering package. Blender Foundation, Stichting Blender Foundation, Amsterdam (2018), http://www.blender.org
2. Bommes, D., Zimmer, H., Kobbelt, L.: Mixed-integer quadrangulation. ACM Transactions on Graphics (TOG) **28**(3) (2009). https://doi.org/10.1145/1531326.1531383
3. Calderon, S., Boubekeur, T.: Bounding proxies for shape approximation. ACM Transactions on Graphics (TOG) **36**(4) (2017)
4. Chen, R., Zhang, J., Liang, Y., Luo, G., Li, W., Liu, J., Li, X., Long, X., Feng, J., Tan, P.: Dora: Sampling and benchmarking for 3d shape variational auto-encoders. In: Proceedings of the IEEE/CVF Conference on Computer Vision and Pattern Recognition. pp. 16251–16261 (2025)
5. Chen, Y., Wang, Y., Luo, Y., Wang, Z., Chen, Z., Zhu, J., Zhang, C., Lin, G.: Meshanything v2: Artist-created mesh generation with adjacent mesh tokenization. In: Proceedings of the IEEE/CVF International Conference on Computer Vision. pp. 13922–13931 (2025)
6. Chen, Z., Tagliasacchi, A., Funkhouser, T., Zhang, H.: Neural dual contouring. ACM Transactions on Graphics (TOG) (2022)
7. Chen, Z., Zhang, H.: Neural marching cubes. ACM Transactions on Graphics (TOG) **40**(6) (2021). https://doi.org/10.1145/3478513.3480518
8. Cousty, J., Bertrand, G., Najman, L., Couprie, M.: Watershed cuts: Minimum spanning forests and the drop of water principle. IEEE Transactions on Pattern Analysis and Machine Intelligence (TPAMI) (2009). https://doi.org/10.1109/TPAMI.2008.173
9. Curless, B., Levoy, M.: A volumetric method for building complex models from range images. In: Proceedings of the 23rd annual conference on Computer graphics and interactive techniques. pp. 303–312 (1996)
10. Dawson-Haggerty, M., et al.: trimesh (2019), https://github.com/mikedh/trimesh
11. Deitke, M., Schwenk, D., Salvador, J., Weihs, L., Michel, O., VanderBilt, E., Schmidt, L., Ehsani, K., Kembhavi, A., Farhadi, A.: Objaverse: A universe of annotated 3d objects. In: Proceedings of the IEEE/CVF conference on computer vision and pattern recognition. pp. 13142–13153 (2023)
12. Dielen, A., Lim, I., Lyon, M., Kobbelt, L.: Learning direction fields for quad mesh generation. Computer Graphics Forum **40**(5) (2021)
13. Dong, Q., Wang, J., Xu, R., Lin, C., Liu, Y., Xin, S., Zhong, Z., Li, X., Tu, C., Komura, T., Kobbelt, L., Schaefer, S., Wang, W.: Crossgen: Learning and generating cross fields for quad meshing. ACM Transactions on Graphics (TOG) **44**(6) (2025). https://doi.org/10.1145/3763299

14. Dong, S., Bremer, P.T., Garland, M., Pascucci, V., Hart, J.C.: Spectral surface quadrangulation. ACM Transactions on Graphics (TOG) **25**(3), 1057–1066 (2006). https://doi.org/10.1145/1141911.1141993
15. Forstmann, S.: Fast quadric mesh simplification (2014), https://github.com/sp4cerat/Fast-Quadric-Mesh-Simplification
16. Gao, D., Siddiqui, Y., Li, L., Dai, A.: Meshart: Generating articulated meshes with structure-guided transformers. In: Proceedings of the Computer Vision and Pattern Recognition Conference. pp. 618–627 (2025)
17. Garland, M., Heckbert, P.S.: Surface simplification using quadric error metrics. In: Proceedings of the 24th annual conference on Computer graphics and interactive techniques. pp. 209–216 (1997)
18. Hao, Z., Romero, D.W., Lin, T.Y., Liu, M.Y.: Meshtron: High-fidelity, artist-like 3d mesh generation at scale. arXiv preprint arXiv:2412.09548 (2024)
19. He, X., Zou, Z.X., Chen, C.H., Guo, Y.C., Liang, D., Yuan, C., Ouyang, W., Cao, Y.P., Li, Y.: Sparseflex: High-resolution and arbitrary-topology 3d shape modeling. In: Proceedings of the IEEE/CVF International Conference on Computer Vision. pp. 14822–14833 (2025)
20. Hoppe, H.: Progressive meshes. In: Proceedings of SIGGRAPH (1996). https://doi.org/10.1145/237170.237216
21. Huang, J., Zhou, Y., Niessner, M., Shewchuk, J.R., Guibas, L.J.: Quadriflow: A scalable and robust method for quadrangulation. In: Computer Graphics Forum. vol. 37, pp. 147–160. Wiley Online Library (2018)
22. Hunyuan3D, T., Yang, S., Yang, M., Feng, Y., Huang, X., Zhang, S., He, Z., Luo, D., Liu, H., Zhao, Y., et al.: Hunyuan3d 2.1: From images to high-fidelity 3d assets with production-ready pbr material. arXiv preprint arXiv:2506.15442 (2025)
23. Jakob, W., Tarini, M., Panozzo, D., Sorkine-Hornung, O.: Instant field-aligned meshes. ACM Transactions on Graphics (Proceedings of SIGGRAPH Asia) **34**(6), 189:1–189:15 (2015). https://doi.org/10.1145/2816795.2818078
24. Ju, T., Losasso, F., Schaefer, S., Warren, J.: Dual contouring of hermite data. ACM Transactions on Graphics (TOG) **21**(3) (2002)
25. Kazhdan, M., Bolitho, M., Hoppe, H.: Poisson surface reconstruction. In: Symposium on Geometry Processing (SGP) (2006)
26. Kazhdan, M., Hoppe, H.: Screened poisson surface reconstruction. ACM Transactions on Graphics (TOG) **32**(3) (2013). https://doi.org/10.1145/2487228.2487237
27. Kerbl, B., Kopanas, G., Leimkühler, T., Drettakis, G.: 3d gaussian splatting for real-time radiance field rendering. ACM Transactions on Graphics **42**(4) (2023). https://doi.org/10.1145/3592433
28. Knöppel, F., Crane, K., Pinkall, U., Schröder, P.: Globally optimal direction fields. ACM Transactions on Graphics (TOG) **32**(4) (2013)
29. Kristof, S.: pyfqmr: Fast Quadric Mesh Reduction for Python (2021), https://github.com/Kramer84/pyfqmr-Fast-Quadric-Mesh-Reduction
30. Li, H., Erkoc, Z., Li, L., Sirigatti, D., Rosov, V., Dai, A., Nießner, M.: Meshpad: Interactive sketch-conditioned artist-reminiscent mesh generation and editing. In: Proceedings of the IEEE/CVF International Conference on Computer Vision. pp. 16227–16237 (2025)
31. Li, W., Liu, J., Yan, H., Chen, R., Liang, Y., Chen, X., Tan, P., Long, X.: Craftsman3d: High-fidelity mesh generation with 3d native generation and interactive geometry refiner. arXiv preprint arXiv:2405.14979 (2024)

32. Li, Y., Zou, Z.X., Liu, Z., Wang, D., Liang, Y., Yu, Z., Liu, X., Guo, Y.C., Liang, D., Ouyang, W., et al.: Triposg: High-fidelity 3d shape synthesis using large-scale rectified flow models. IEEE Transactions on Pattern Analysis and Machine Intelligence (2025)
33. Lionar, S., Liang, J., Lee, G.H.: Treemeshgpt: Artistic mesh generation with autoregressive tree sequencing. In: Proceedings of the Computer Vision and Pattern Recognition Conference. pp. 26608–26617 (2025)
34. Lipman, Y., Chen, R.T.Q., Ben-Hamu, H., Nickel, M., Le, M.: Flow matching for generative modeling. arXiv preprint arXiv:2210.02747 (2022)
35. Liu, M., Uy, M.A., Xiang, D., Su, H., Fidler, S., Sharp, N., Gao, J.: Partfield: Learning 3d feature fields for part segmentation and beyond. In: Proceedings of the IEEE/CVF International Conference on Computer Vision. pp. 9704–9715 (2025)
36. Liu, X., Gong, C., Liu, Q.: Flow straight and fast: Learning to generate and transfer data with rectified flow. arXiv preprint arXiv:2209.03003 (2022)
37. Liu, Y.T., Li, J., Liu, Y.T., Yu, X., Guo, Y.C., Cao, Y.P., Liang, D., Shamir, A., Zhang, S.H.: Neuframeq: Neural frame fields for scalable and generalizable anisotropic quadrangulation. In: Proceedings of the IEEE/CVF International Conference on Computer Vision. pp. 28000–28009 (2025)
38. Lorensen, W.E., Cline, H.E.: Marching cubes: A high resolution 3d surface construction algorithm. In: Seminal graphics: pioneering efforts that shaped the field, pp. 347–353 (1998)
39. Mangan, A.P., Whitaker, R.T.: Partitioning 3d surface meshes using watershed segmentation. IEEE Transactions on Visualization and Computer Graphics (TVCG) **5**(4), 308–321 (1999)
40. Mescheder, L., Oechsle, M., Niemeyer, M., Nowozin, S., Geiger, A.: Occupancy networks: Learning 3d reconstruction in function space. In: Proceedings of the IEEE/CVF Conference on Computer Vision and Pattern Recognition (CVPR) (2019). `https://doi.org/10.1109/CVPR.2019.00459`
41. MeshLib: Geometry processing library (2025), `https://meshlib.io`
42. Mildenhall, B., Srinivasan, P.P., Tancik, M., Barron, J.T., Ramamoorthi, R., Ng, R.: Nerf: Representing scenes as neural radiance fields for view synthesis. In: Proceedings of the European Conference on Computer Vision (ECCV) (2020)
43. Nash, C., Ganin, Y., Eslami, S.M.A., Battaglia, P.W.: Polygen: An autoregressive generative model of 3d meshes. In: Proceedings of the International Conference on Machine Learning (ICML) (2020)
44. Newcombe, R.A., Izadi, S., Hilliges, O., Molyneaux, D., Kim, D., Davison, A.J., Kohli, P., Shotton, J., Hodges, S., Fitzgibbon, A.: Kinectfusion: Real-time dense surface mapping and tracking. In: Proceedings of the IEEE International Symposium on Mixed and Augmented Reality (ISMAR). pp. 127–136 (2011). `https://doi.org/10.1109/ISMAR.2011.6092378`
45. Nießner, M., Zollhöfer, M., Izadi, S., Stamminger, M.: Real-time 3d reconstruction at scale using voxel hashing. ACM Transactions on Graphics (TOG) **32**(6) (2013). `https://doi.org/10.1145/2508363.2508374`
46. Palacios, J., Zhang, E.: Rotational symmetry field design on surfaces. ACM Transactions on Graphics (TOG) **26**(3) (2007)
47. Park, J.J., Florence, P., Straub, J., Newcombe, R., Lovegrove, S.: Deepsdf: Learning continuous signed distance functions for shape representation. In: Proceedings of the IEEE/CVF conference on computer vision and pattern recognition. pp. 165–174 (2019)
48. Salinas, D., Lafarge, F., Alliez, P.: Structure-aware mesh decimation. In: Computer Graphics Forum. vol. 34, pp. 211–227. Wiley Online Library (2015)

49. Shen, T., Gao, J., Yin, K., Liu, M.Y., Fidler, S.: Deep marching tetrahedra: a hybrid representation for high-resolution 3d shape synthesis. In: Advances in Neural Information Processing Systems (NeurIPS) (2021)
50. Shen, T., Munkberg, J., Hasselgren, J., Yin, K., Wang, Z., Chen, W., Gojcic, Z., Fidler, S., Sharp, N., Gao, J.: Flexible isosurface extraction for gradient-based mesh optimization. ACM Transactions on Graphics (TOG) **42**(4) (2023). https://doi.org/10.1145/3592430
51. Siddiqui, Y., Alliegro, A., Artemov, A., Tommasi, T., Sirigatti, D., Rosov, V., Dai, A., Nießner, M.: Meshgpt: Generating triangle meshes with decoder-only transformers. In: Proceedings of the IEEE/CVF conference on computer vision and pattern recognition. pp. 19615–19625 (2024)
52. Tang, J.: Meshiki: A collection of unusual mesh processing algorithms (2025), https://github.com/ashawkey/meshiki
53. Tang, J., Li, Z., Hao, Z., Liu, X., Zeng, G., Liu, M.Y., Zhang, Q.: Edgerunner: Auto-regressive auto-encoder for artistic mesh generation. arXiv preprint arXiv:2409.18114 (2024)
54. Team, G., Anil, R., Borgeaud, S., Alayrac, J.B., Yu, J., Soricut, R., Schalkwyk, J., Dai, A.M., Hauth, A., Millican, K., et al.: Gemini: a family of highly capable multimodal models. arXiv preprint arXiv:2312.11805 (2023)
55. Team, Q.: Qwen3.5: Accelerating productivity with native multimodal agents (February 2026), https://qwen.ai/blog?id=qwen3.5
56. Tong, A., Malkin, N., Huguet, G., Zhang, Y., Rector-Brooks, J., Fatras, K., Wolf, G., Bengio, Y.: Conditional flow matching: Simulation-free dynamic optimal transport. arXiv preprint arXiv:2302.00482 (2023)
57. Trettner, P., Kobbelt, L.: Fast and robust qef minimization using probabilistic quadrics. In: Computer Graphics Forum. vol. 39, pp. 325–334. Wiley Online Library (2020)
58. Vincent, L., Soille, P.: Watersheds in digital spaces: An efficient algorithm based on immersion simulations. IEEE Transactions on Pattern Analysis and Machine Intelligence (TPAMI) (1991). https://doi.org/10.1109/34.87344
59. Wang, P., Liu, L., Liu, Y., Theobalt, C., Komura, T., Wang, W.: Neus: Learning neural implicit surfaces by volume rendering for multi-view reconstruction. In: Advances in Neural Information Processing Systems (NeurIPS). pp. 27171–27183 (2021)
60. Wang, Y., Yi, X., Weng, H., Xu, Q., Wei, X., Yang, X., Guo, C., Chen, L., Zhang, H.: Nautilus: Locality-aware autoencoder for scalable mesh generation. In: Proceedings of the IEEE/CVF International Conference on Computer Vision. pp. 10961–10970 (2025)
61. Wu, S., Lin, Y., Zhang, F., Zeng, Y., Yang, Y., Bao, Y., Qian, J., Zhu, S., Cao, X., Torr, P., et al.: Direct3d-s2: Gigascale 3d generation made easy with spatial sparse attention. arXiv preprint arXiv:2505.17412 (2025)
62. Wu, T., Yang, G., Li, Z., Zhang, K., Liu, Z., Guibas, L., Lin, D., Wetzstein, G.: Gpt-4v (ision) is a human-aligned evaluator for text-to-3d generation. In: Proceedings of the IEEE/CVF conference on computer vision and pattern recognition. pp. 22227–22238 (2024)
63. Xiang, J., Chen, X., Xu, S., Wang, R., Lv, Z., Deng, Y., Zhu, H., Dong, Y., Zhao, H., Yuan, N.J., et al.: Native and compact structured latents for 3d generation. arXiv preprint arXiv:2512.14692 (2025)
64. Xiang, J., Lv, Z., Xu, S., Deng, Y., Wang, R., Zhang, B., Chen, D., Tong, X., Yang, J.: Structured 3d latents for scalable and versatile 3d generation. In: Proceedings

of the IEEE/CVF conference on computer vision and pattern recognition. pp. 21469–21480 (2025)
65. Xu, R., Xue, T., Dong, Q., Wan, L., Zhu, Z., Li, P., Dou, Z., Lin, C., Xin, S., Liu, Y., et al.: Meshmosaic: Scaling artist mesh generation via local-to-global assembly. arXiv preprint arXiv:2509.19995 (2025)
66. Ye, C., Wu, Y., Lu, Z., Chang, J., Guo, X., Zhou, J., Zhao, H., Han, X.: Hi3dgen: High-fidelity 3d geometry generation from images via normal bridging. In: Proceedings of the IEEE/CVF International Conference on Computer Vision. pp. 25050–25061 (2025)
67. Zhang, X., Siddiqui, Y., Avetisyan, A., Xie, C., Engel, J., Howard-Jenkins, H.: Vertexregen: Mesh generation with continuous level of detail. In: Proceedings of the IEEE/CVF International Conference on Computer Vision. pp. 12570–12580 (2025)
68. Zhao, R., Ye, J., Wang, Z., Liu, G., Chen, Y., Wang, Y., Zhu, J.: Deepmesh: Auto-regressive artist-mesh creation with reinforcement learning. In: Proceedings of the IEEE/CVF International Conference on Computer Vision. pp. 10612–10623 (2025)
69. Zhao, T., Busé, L., Cohen-Steiner, D., Boubekeur, T., Thiery, J.M., Alliez, P.: Variational shape reconstruction via quadric error metrics. In: ACM SIGGRAPH 2023 conference proceedings. pp. 1–10 (2023)
70. Zhou, Q.Y., Park, J., Koltun, V.: Open3D: A modern library for 3D data processing. arXiv:1801.09847 (2018)

Appendix

In this material, we provide extended technical details, implementation details, and additional experimental results. In Sec. A, we describe our data filtering pipeline and the mathematical formulation of the distortion fields used for data augmentation. Sec. B demonstrates TriFlow's generalization to meshes produced by vecset-based 3D generators, and Sec. C discusses scaling TriFlow to higher voxelization resolutions. Subsequently, Sec. D details the implementation in training, mesh extraction, and perceptual study. Sec. E provides additional experimental statistics, including a runtime breakdown and topological validity metrics compared to existing baselines. Finally, Sec. F presents ablation studies regarding our NVF parameterization, the robustness of the root threshold τ, quad ratio, and the topology weight λ_t.

A Data Filtering and Augmentation Details

Data Filtering. Although the NVF is defined on the surface of a geometry, the latent generative model relies on voxelization, which assumes a well-defined intersection-free surface. In practice, this assumption may not hold. Modern 3D modeling pipelines typically construct assets from multiple parts that are assembled together, leading to triangle intersections or overlapping surfaces near part boundaries. Such artifacts introduce ambiguities during voxelization and are undesirable for training. To mitigate this issue, we decompose each object into connected components and treat each component as an independent training sample.

Since Objaverse contains many non-artist-created meshes, we apply additional filtering to maximize the training data quality. First, we collapse all mesh edges shorter than the voxel diagonal; samples requiring more than 50% triangle reduction during this process are discarded to ensure topological integrity. To exclude excessively thin or elongated geometries, we remove meshes with fewer than 40k occupied voxels at the resolution of 512^3. Furthermore, we filter for mesh regularity by discarding samples with a quad face ratio below 50%. Since Objaverse contains diverse mesh types (e.g., polygonal and triangulated), we unify this metric by first triangulating all meshes and then using Meshiki [52] to estimate the proportion of triangle pairs forming quads. In this context, the quad ratio serves as a proxy for the regularity of triangle alignment rather than a precise count of polygonal faces.

Data Augmentation. Topology generation is frequently applied to imperfect geometry containing local distortions, as commonly observed in scanned or generated meshes. To improve robustness, we apply a random distortion field $\boldsymbol{\delta} : \mathbb{R}^3 \to \mathbb{R}^3$ that defines a continuous deformation in 3D space. For a vertex $\boldsymbol{p}$, the displacement is given by

$$\boldsymbol{\delta}(\boldsymbol{p}) = \left[1 - \exp\left(-\frac{\|\boldsymbol{p} - \boldsymbol{v}_n\|_2^2}{2r_s^2}\right)\right] \sum_{i=1}^{M} w_i \left(\frac{\|\boldsymbol{p} - \boldsymbol{a}_i\|_2}{r_a}\right) \boldsymbol{d}_i, \tag{A.1}$$

Algorithm A.1 Priority Watershed NVF Refinement on Dense Mesh

Require: Over-tessellated mesh $\mathcal{M}_d = (\mathcal{V}_d, \mathcal{F}_d)$, predicted NVF $\boldsymbol{t}_d(\boldsymbol{v}_d)$, threshold τ
Initialize all vertices as unlabeled
Root initialization $\mathcal{R} = \{\boldsymbol{r} \in \mathcal{V}_d \mid \|\boldsymbol{t}_d(\boldsymbol{r})\|_\infty \leq \tau\}$ ▷ Eq. (6)
for $\boldsymbol{r} \in \mathcal{R}$ **do** ▷ Initialize priority queue
    Push $(0, \boldsymbol{r}, \boldsymbol{r})$
end for
while priority queue not empty **do** ▷ Iterative region expansion
    Pop $(\text{cost}, \boldsymbol{u}, \boldsymbol{r})$ with smallest cost
    if $\boldsymbol{u}$ already labeled **then**
        continue
    end if
    Assign vertex $\boldsymbol{u}$ to root $\boldsymbol{r}$
    for $\boldsymbol{v} \in \text{Neighbor}(\boldsymbol{u}, \mathcal{M}_d)$ **do**
        if $\boldsymbol{v}$ unlabeled **then**
            Push $(\text{cost}(\boldsymbol{v}, \boldsymbol{r}), \boldsymbol{v}, \boldsymbol{r})$ ▷ Eq. (7)
        end if
    end for
end while
Update NVF ▷ Eq. (8)

where $\boldsymbol{v}_n$ is the closest vertex of the original mesh to $\boldsymbol{p}$, r_s is a static falloff radius controlling how strongly regions near the original mesh vertices are preserved, and r_a is an anchor radius that determines the spatial extent of its influence. $\{\boldsymbol{a}_i\}_{i=1}^M$ are control points with associated displacements $\{\boldsymbol{d}_i\}_{i=1}^M$, and $w_i(r)$ is the Wendland C2 weighting function:

$$w_i(r) = \begin{cases} (1-r)^4(4r+1), & r < 1, \\ 0, & r \geq 1. \end{cases} \tag{A.2}$$

The distorted NVF is defined consistently by applying the deformation to both query points and their corresponding target vertices:

$$\boldsymbol{t}_\delta(\delta(\boldsymbol{p})) = \delta(\boldsymbol{v}_n) - \delta(\boldsymbol{p}). \tag{A.3}$$

In practice, the static falloff scales the displacement according to the proximity to the vertices of the original mesh. As a result, regions with denser triangles experience smaller perturbations, whereas sparser regions are distorted more strongly. This ensures that the model learns to preserve fine geometric details when generating high-resolution meshes, while being able to simplify geometry effectively when targeting coarser meshes with fewer triangles.

B Generalization to Vecset Generative Models

Beyond geometries produced by voxel-based generative models such as TRELLIS [64], we test TriFlow on outputs of vecset-based generators. Because TriFlow operates on the SDF of its input, applying it to vecset outputs requires no

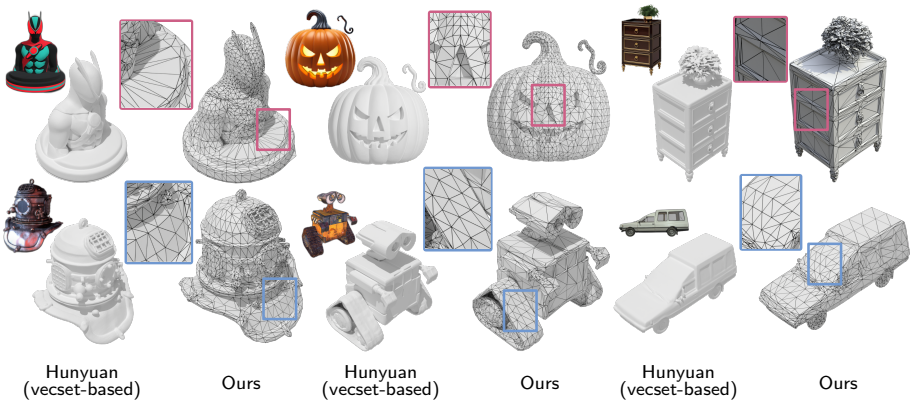


Fig. A.1: TriFlow generalizes to meshes produced by the vecset-based 3D generator Hunyuan3D-2.1 [22].

changes to the model. Fig. A.1 shows TriFlow retopologizing meshes generated by Hunyuan3D-2.1 [22]. TriFlow is trained exclusively on Objaverse artist-authored meshes, yet produces compact, artist-like triangle layouts on both voxel- and vecset-generated inputs, suggesting that the NVF representation transfers across upstream generator families.

C Scaling to Higher Resolution

The NVF is defined on the surface and is resolution-independent. In practice, however, our training pipeline voxelizes the field, which sets a lower bound on the size of triangles that can be reliably reconstructed: small features embedded in otherwise smooth regions, such as the whale's eye in Fig. A.2, collapse when their triangle footprints approach the voxel grid spacing, and the bound recedes proportionally with resolution. Scaling the voxelization from 512^3 to 1024^3 halves the spacing and pushes this bound down accordingly, recovering features that were previously unreachable.

The NVF formulation is independent of voxel resolution; the 512^3 choice in the main paper reflects our training budget rather than a representational limit. As a proof of concept, we fine-tune the NVF VAE and the flow model to 1024^3 using the same positional-encoding-frequency-rescaling technique adopted by TRELLIS [64] and Direct3D-S2 [61] for high-resolution training. On a held-out set of $\sim$150 dense Objaverse meshes, the fine-tuned 1024^3 NVF VAE achieves a mean directional cosine similarity of 0.996 and an ℓ_2 error of 5.46×10^{-4}, compared to 0.888 and 2.41×10^{-3} for the original 512^3 NVF VAE evaluated on the same set. Fig. A.2 shows representative qualitative results: TriFlow preserves fine-grained topology that is unreachable at 512^3.

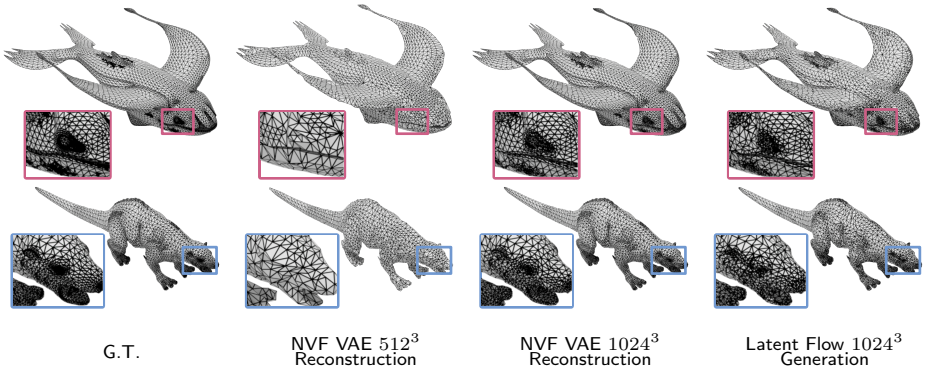


Fig. A.2: TriFlow preserves fine-grained topology at higher resolutions, after fine-tuning on ∼150 dense meshes at 1024^3.

D Additional Implementation Details

Training. The NVF VAE is adapted from Direct3D-S2's SDF VAE [61]. The decoder prunes empty regions using the sparse voxel coordinates of the input after each up-sampling layer, allowing memory-efficient training. We change the hidden dimensions in the decoder from $(512, 128, 64, 32)$ to $(1024, 512, 256, 256)$ to capture the details of the NVF.

During training, low- and high-frequency displacement fields are applied on meshes normalized to a unit cube. Low-frequency distortion uses 32 anchor points with $r_s = 0.5$ with displacements of length $1/1024$. High-frequency distortion uses 64 anchors with $r_s = 1/8$ with displacements of length $1/512$. The r_a is set to $1/8$.

Implementation. Dataset filtering, pre-processing, and NVF computation are implemented using Trimesh [10], MeshLib [41], Open3D [70], and Meshiki [52]. The NVF post-processing, including bilateral filtering and the watershed algorithm, are implemented in Python, while the constrained QEM is implemented based on Fast-QEM [15, 29] in C++. We provide the details of the watershed algorithm in Alg. A.1.

In practice, we relax the constraint in the QEM by allowing contractions between nearby vertices within a small spatial threshold, even when their roots differ, provided that the operation does not split an existing region into multiple disconnected components. Furthermore, collapses that introduce non-manifold edges are rejected to maintain mesh validity and to prevent root vertices from becoming disconnected from the mesh.

Perceptual Study. The perceptual study for both VLMs and human participants follows the same setting. In the unary study, participants are shown wireframe renderings of each method and asked to rate the geometric similarity and the topological quality on a scale of 1 (poor) to 5 (excellent). In the binary study, participants are shown the results of two methods side-by-side and asked to independently choose the one with better geometry preservation, higher topology

Table A.1: Additional Statistics. NE stands for the ratio of non-manifold edges. Compared to learning-based methods [33, 65], our method has significantly reduced topological error and fast inference, achieving topology validity and speed comparable to classical baselines [17, 21].

Method	Objaverse				TRELLIS			
	NE↓	#Face	#Components↓	Time/s↓	NE↓	#Face	#Components↓	Time/s↓
QEM [17]	0.3‰	1132	1.1	22	0.1‰	6154	**1.0**	**26**
QuadriFlow [21]	**0.1‰**	833	**1.0**	20	0.1‰	4610	2.5	31
MeshMosaic [65]	8.6‰	1563	51.6	66	8.7‰	95297	1493.8	7813
TreeMeshGPT [33]	1.0‰	1606	5.6	57	4.0‰	6999	36.1	258
Ours	**0.1‰**	1146	1.1	**15**	**0.0‰**	6154	**1.0**	31

Table A.2: Ablation on NVF parameterizations. All models are trained for 20k iterations, showing that the performance difference is already distinguishable at the early stage of training. The reported metrics include the synthesized NVF's ℓ_2 distance $\ell_2(\boldsymbol{t})$, directional cosine similarity $\cos_{\boldsymbol{d}}$, ℓ_1 error of the length $\ell_1(\|\boldsymbol{t}\|_2)$, and ℓ_2 distance of target positions $\ell_2(\boldsymbol{x})$, which shows numerically the accuracy of the prediction. Our parameterization using direction and square root length outperforms other parameterizations.

Method	$\boldsymbol{\ell_2(t)}\downarrow$	$\boldsymbol{\cos_d}\uparrow$	$\boldsymbol{\ell_1(\|t\|_2)}\downarrow$	$\boldsymbol{\ell_2(x)}\downarrow$
Parameterize w/ vectors	0.14	0.17	0.07	0.14
Parameterize w/ target positions	0.16	0.16	0.09	0.14
Ours	**0.10**	**0.26**	**0.06**	**0.11**

regularity, and overall preference. The VLM evaluations are conducted using Qwen-3.5-Plus [55] and Gemini-3-Flash [54] with around 1700 queries in total. Furthermore, we collected 357 effective human responses for the unary perceptual study and 622 for the binary perceptual study from 33 human participants. We observe that the human evaluations align closely with VLMs, as shown in Tabs. 1 and 2, highlighting the reliability of both evaluations.

Our VLM prompting adapts the GPTEval3D [62] to mesh wireframe comparisons, with method order randomized across queries to avoid positional bias. Full prompts are provided in Prompts A.1 and A.2.

E Additional Experimental Statistics

In Sec. 4.4, we report perceptual ratings and preference on the output meshes, which reflect the visual geometry similarities of the shaded renderings and regularities of the wireframe renderings in human preference. We further report topological statistics, including the ratio of non-manifold edges, the number of faces, and the number of disconnected components, along with runtime, in Tab. A.1, demonstrating the topological validity and computational efficiency of these methods. The result demonstrates that TriFlow outperforms learning-based baselines [33, 65] by achieving fewer non-manifold edges and components,

as well as more than 8× inference speedup. Generally, TriFlow has the same performance level as classical baselines [17, 21] but generates artist-like topology that is better suited for production (Sec. 4.4). By defining the topology as NVF, TriFlow not only achieves higher generation speed, but also benefits from existing optimization paradigms in QEM with fewer topological errors.

Runtime breakdown. On average, the flow-matching procedure, involving 50 denosing steps, occupies 22.8% of the processing time. The bilateral filtering takes 12.7%. The watershed algorithm takes 37.3%. Finally, the constrained QEM takes 18.7%. The rest 8.5% is mainly the cost of memory allocations for the NVF. Note that we adapt Fast-QEM [15] in our implementation, which compromises accuracy for speed. Therefore, the runtime of our QEM is lower than the baseline QEM, which has higher accuracy. Our bilateral and watershed methods are implemented in Python, which are not fully optimized for speed. Further improvement with parallel processing is an interesting future avenue to explore.

F Additional Ablations

Our parameterization of the NVF enables efficient learning. We highlight in Sec. 3.2 that we parameterize the NVF as $(\boldsymbol{d}, s)$, which is the direction and square root of the length of the vector. We conduct an ablation study with two variants: using directly the NVF $\boldsymbol{t}(\boldsymbol{v})$, and using target positions $\boldsymbol{x}(\boldsymbol{v}) = \boldsymbol{v} + \boldsymbol{t}(\boldsymbol{v})$. We report the synthesized NVF's ℓ_2 distance $\ell_2(\boldsymbol{t})$, directional cosine similarity $\cos_{\boldsymbol{d}}$, ℓ_1 error of the length $\ell_1(\|\boldsymbol{t}\|_2)$, and ℓ_2 distance of target positions $\ell_2(\boldsymbol{x})$. The networks are flow-matching models (w/o latent) trained at a resolution of 128^3. As shown in Tab. A.2, our chosen parameterization achieves significantly improved prediction accuracy, already in the early stage of the training.

Our mesh extraction is robust to variations in the root threshold τ. In Fig. A.3, we demonstrate the impact of different τ values during watershed root initialization. When τ is set too low, essential roots are not identified; in the extreme case of $\tau = 0$, the entire surface area collapses into a single cluster, failing to reflect the topology implicit in the NVF. Conversely, a high τ value over-segments the surface into redundant subgroups that share the same target vertex. However, by allowing the merging of spatially proximal vertices across different clusters (see Sec. D), the pipeline remains robust to this over-segmentation. As shown in Fig. A.3, the resulting mesh closely matches the NVF even in the extreme case of $\tau = 10$ voxel size. In practice, we recommend $\tau = 1/2$ voxel size, or slightly larger, to ensure all primary groups are captured while minimizing unnecessary subdivisions.

The quad ratio acts as an effective filter for irregular topology. As discussed in Sec. A, the quad ratio serves as a proxy for the regularity of triangle arrangements. Consequently, enforcing a higher quad ratio leads to more structured and regular mesh topologies, as illustrated in Fig. A.4. This condition serves as a sink for poor topology, allowing the model to be trained on a larger variety of samples without being affected by their topological defects.

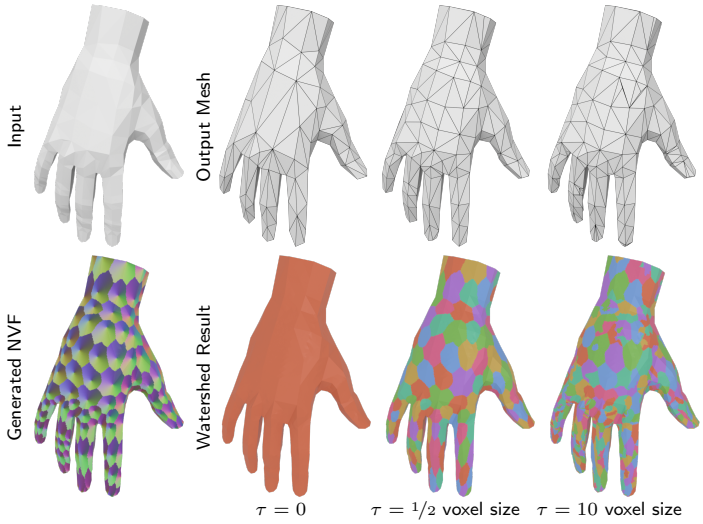


Fig. A.3: Ablation study on root threshold τ. A low threshold clusters the entire surface into a single group, causing the mesh topology to diverge from the generated NVF. Conversely, a high threshold creates redundant surface regions where multiple clusters share the same target vertex. By allowing the QEM simplification to merge spatially close vertices from different clusters, the process becomes more robust to variations in τ. Even at a high value of $\tau = 10$ voxel size, the resulting topology remains largely aligned with the NVF prediction.

A small topology weight λ_t effectively snaps vertices to target positions. As illustrated in Fig. A.5, even a small weight of $\lambda_t = 0.1$ is sufficient to align the output mesh vertices with the structural features, such as the centerline of the chair. This parameter exhibits significant robustness, as the output mesh remains topologically reasonable even when the weight is increased to $\lambda_t = 10$. In our experiments, we set $\lambda_t = 0.1$; this value effectively enforces alignment to the NVF without overpowering the geometric fidelity constraints from the vanilla QEM formulation.

Prompt A.1: Unary VLM evaluation prompt

Task Description
You are an expert 3D Technical Artist. Your task is to evaluate 3D reconstruction methods by comparing their output meshes against a reference input (far left).
Instructions
Scope: Identify the input and all present reconstruction methods (A, B, C...).
Observation: Closely examine the wireframe. Do not be misled by low-polygon counts; look for the logic of the edge placement.
Independence of Criteria: Treat Geometry and Topology as separate scores. A model can have perfect shape but terrible topology, or vice versa.

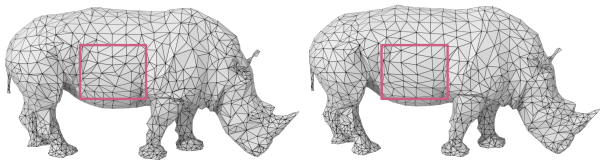


Fig. A.4: Ablation study on target quad ratio. Reducing the target quad ratio results in a less regular triangle arrangement, leading to fewer triangle pairs that form quads.

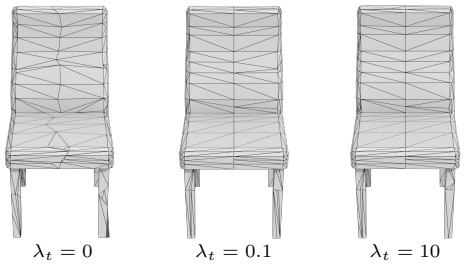


Fig. A.5: Ablation study on topology weight λ_t. With $\lambda_t = 0$, the contraction points are not aligned to the NVF prediction, resulting in undesired vertex placements. With a small $\lambda_t = 0.1$, the vertices align with the centerline of the chair, which is identical to an intense weight $\lambda_t = 10$.

Review the input mesh: When you consider the method, you need to look again at the input mesh to have better and consistent scoring. This also means that the order of the methods shouldn't affect the scoring and you should not consider other methods when grading the current method.
Evaluation Criteria
CRITERIA 1: SHAPE PRESERVATION AND STRUCTURAL INTEGRITY
Score 1 (Failure): The mesh exhibits major structural failure. There are significant holes, often indicated by dark or black rendering artifacts where light cannot calculate correctly. The geometry is likely non-manifold, missing entire faces, or consists of disconnected components that should be solid.
Score 2 (Poor): There is significant loss of volume or silhouette. Critical thin structures, such as pipes, railings, or antennas, are deleted, severely broken, or floating as disconnected debris. Large gaps may be present in the mesh, preventing it from being watertight.
Score 3 (Average): The general volume of the object is preserved, but thin structures appear crumbly, jagged, or distorted. Surface continuity is acceptable, but sharp features are often over-smoothed or eroded. The object looks like a melted version of the input.
Score 4 (Good): The mesh is watertight with no dark hole artifacts. Most features are preserved. There is minor simplification of thin structures, but they remain connected and coherent. The silhouette matches the input closely.

Score 5 (Excellent): The mesh is perfectly watertight and structurally complete. Thin structures like cables, railings, or mechanical parts are distinct, straight, and continuous. Sharp hard-surface features are crisp. Simplification occurs only on redundant flat areas, never compromising the structural silhouette.
CRITERIA 2: TOPOLOGY LIKENESS TO ARTIST/CAD MESHES
Note on silver triangles: silver triangles (long, thin triangles) are characteristic of CAD-style hard-surface meshing and are a positive signal on those subjects; on organic subjects, they should not be expected.
Score 1 (Unusable): The topology is unusable for professional workflows. It is either a hyper-dense uniform grid (voxel-style) that is impossible to edit, or it creates broken, non-manifold geometry with inverted normals.
Score 2 (Chaotic): The mesh features randomized triangulation. Edges do not follow the geometry's feature lines, resulting in jagged edges on what should be straight objects. Random star poles and noisy clusters of triangles appear on flat surfaces without logic.
Score 3 (Automated Decimation): This represents standard automated decimation. While it reduces polygon count and is technically adaptive (more triangles on curves than flats), the triangulation is noisy. Edges cross flat planes at random angles, and there is no attempt to align edges with the model's axes. It is difficult to UV map or select "loops."
Score 4 (Advanced/Structural Topology): The method shows intentional edge flow. Beyond just being adaptive, the edges start to align with the primary feature lines of the object. Flat areas are mostly clean, and curved sections show the beginnings of organized "strips" or "rings." It avoids the "shattered glass" look of basic decimation, though it may still lack the refinement of a CAD-style hard-surface mesh.
Score 5 (Artist/CAD Standard): The topology is adaptive and mimics a professional human artist. Flat planar surfaces are represented by large triangles with intentionally less compact wireframes to form connected edge loops. Edges align with the geometry's primary feature lines and the mechanical axes of the object. For CAD-style hard-surface subjects, silver triangles are a positive signal of efficient curved-surface representation.
Output Format
Detected Methods: [List all identified methods]
Analysis: Method [Label]:
Shape Preservation: [Brief summary of shape accuracy] Score: [1-5]
Topology: [Note specific areas of "Intentional Flow" (e.g. tracks, beams) vs "Structural Noise." Evaluate if the mesh respects mechanical axes.] Score: [1-5]
Summary Table:
Method	Shape Preservation	Topology
:—	:—	:—
[Label]	[Score]	[Score]

Prompt A.2: Binary (pairwise) VLM evaluation prompt

Our task here is to compare two 3D objects, both generated from the same input reference mesh.
We want to decide which one is better according to the provided criteria.
Instruction
You will see an image containing renderings of the input reference and these two 3D objects.
The left part of the image contains a single-view rendering of the reference shape. The middle part of the image contains a single-view rendering of 3D object 1, with triangle edges (wireframe) colored black, and the right part contains a single-view rendering for 3D object 2, with triangle edges (wireframe) colored black.
We would like to compare these two 3D objects from the following aspects:
1. Artist-involved Topology. This evaluates how alike the mesh triangles are to a human-created mesh. Please consider symmetry, edge flow, and adaptive density. A topology featuring an uninorm grid structure should be flagged as non-artistic due to a lack of adaptive density. CAD converted meshes usually contain long silver triangles, but should be considered an artist mesh. Silver triangles are characteristic of CAD-style hard-surface meshing; on organic subjects, they should not be expected. Low-poly meshes should be considered artist meshes and could be identified by looking at regular regions to see how the edges are aligned. When you consider topology, you should also pay more attention to large clean areas where you will see the edges more clearly, due to the resolution of the image, looking at dense regions might mislead your judgment.
2. Shape Preservation (Geometry). This evaluates how well the reconstruction preserves the physical volume, proportions, and sharp features of the Input. Please first describe each of the two models, and find all missing geometry and broken surface, then evaluate how well it covers ALL the structures in the original input shape.
3. Professional Preference. This shows your personal preference as a professional artist. For each of the object, consider how likely you will use it as an asset in video games, movie production, and to do manual editing in professional 3D softwares.
Take a really close look at each of the single-view images for these two 3D objects and the input mesh before providing your answer.
When evaluating these aspects, focus on one of them and the input mesh at a time.
Try to make independent decision between these criteria.
Output format
To provide an answer, please provide a short analysis for each of the aforementioned evaluation criteria.
The analysis should be very concise and accurate.
For each of the criteria, you need to make a decision using these three options:
1. object 1 is better;
2. object 2 is better;
3. Cannot decide.
PLEASE CONSIDER OPTION 3 IF THE DIFFERENCE IS LESS THAN 10
And then, in the last row, summarize your final decision by "<option for criteria 1> <option for criteria 2> <option for criteria 3>".

An example output looks like follows:
" Analysis:
1. Artist-involved Topology (Wireframe Logic): Object 1 xxxx; Object 2 xxxx;
Object 1/2 is better or cannot decide
2. Shape Preservation (Geometry): Object 1 xxxx; Object 2 xxxx;
Object 1/2 is better or cannot decide
3. Professional Preference. Object 1 xxxx; Object 2 xxxx;
Object 1/2 is better or cannot decide
Final answer:
x x x (e.g., 1 2 2 / 3 3 3 / 3 2 2) "